

## Article

# Ni/Zn Layered Double Hydroxide (LDH) Micro/Nanosystems and Their Azorubine Adsorption Performance

Assia Nait-Merzoug<sup>1,2,\*</sup>, Ouanassa Guellati<sup>1,2,\*</sup>, Salma Djaber<sup>2</sup>, Naima Habib<sup>1,2</sup>, Aicha Harat<sup>1</sup>, Jamal El-Haskouri<sup>3</sup>, Dominique Begin<sup>4</sup> and Mohamed Guerioune<sup>1</sup>

- <sup>1</sup> Laboratoire d'Etude et de Recherche des Etats Condensés (LEREC), Département de Physique, Université Badji-Mokhtar de Annaba, B.P. 12, Annaba 23000, Algeria; [habib.naima23@gmail.com](mailto:habib.naima23@gmail.com) (N.H.); [harat\\_aicha@yahoo.fr](mailto:harat_aicha@yahoo.fr) (A.H.); [mguerioune@yahoo.fr](mailto:mguerioune@yahoo.fr) (M.G.)
- <sup>2</sup> Faculty of Science and Technology, Université Mohamed Chérif Messaadia de Souk-Ahras, B.P. 1553, Souk-Ahras 41000, Algeria; [djaspers669@gmail.com](mailto:djaspers669@gmail.com)
- <sup>3</sup> Institut of Material Science (ICMUV), Universitat de València, Catedrático José Beltrán 2, Paterna, 46980 Valencia, Spain; [Jamal.Haskouri@uv.es](mailto:Jamal.Haskouri@uv.es)
- <sup>4</sup> Institut de Chimie et Procédés pour l'Energie, l'Environnement et la Santé (ICPEES)—ECPM—CNRS—Uds, 25 rue Becquerel, CEDEX 2, 67087 Strasbourg, France; [dominique.begin@unistra.fr](mailto:dominique.begin@unistra.fr)
- \* Correspondence: [abenlala@yahoo.fr](mailto:abenlala@yahoo.fr) (A.N.-M.); [guellati23@yahoo.fr](mailto:guellati23@yahoo.fr) (O.G.)

**Abstract:** A membranous shaped Ni/Zn layered double hydroxide based nano hybrid was obtained using a low-cost template-free hydrothermal process at optimized growth conditions of 180 °C for 6 h. The synthesized nano hybrid was structurally, texturally and morphologically characterized using different techniques such as X-ray diffraction, FTIR, XPS spectroscopy, BET analysis and FESEM microscopy. The adsorption performance of our product was estimated through the Azorubine dye removal from synthetic wastewater. We therefore studied the synergic effects of Ni/Zn adsorbent dosage, contact time, pH, adsorbate concentration, stirring speed and temperature on the Azorubine adsorption efficiency. In this investigation, we obtained bi-structure based nano adsorbent with 54% crystallinity order composed of nickel hydrate and zinc carbonate hydroxides in irregular nanoflake-like mesoporous nano hybrid morphology. Interestingly, it was also revealed to have high specific surface area (SSA) of around 110 m<sup>2</sup> g<sup>-1</sup> with important textural properties of 18 nm and 0.68 cm<sup>3</sup> g<sup>-1</sup> average pore size and volume, respectively. Moreover, the adsorption results revealed that this novel Ni/Zn layered double hydroxide (Ni/Zn LDH) was an efficient adsorbent for Az molecule and possesses an adsorptive ability exhibiting a short equilibrium time (60 min) and a high Az adsorption capability (223 mg g<sup>-1</sup>). This fast removal efficiency was attributed to high contact surface area via mesoporous active sites accompanied with the presence of functional groups (OH<sup>-</sup> and CO<sub>3</sub><sup>2-</sup>). In addition, the Langmuir and Freundlich isotherms were studied, and the results fitted better to the Langmuir isotherm.

**Keywords:** Ni/Zn layered double hydroxide; Azorubine; adsorption; nano hybrid; Carmoisine



**Citation:** Nait-Merzoug, A.; Guellati, O.; Djaber, S.; Habib, N.; Harat, A.; El-Haskouri, J.; Begin, D.; Guerioune, M. Ni/Zn Layered Double Hydroxide (LDH) Micro/Nanosystems and Their Azorubine Adsorption Performance. *Appl. Sci.* **2021**, *11*, 8899. <https://doi.org/10.3390/app11198899>

Academic Editor: Jong-Wan Hu

Received: 15 August 2021

Accepted: 16 September 2021

Published: 24 September 2021

**Publisher's Note:** MDPI stays neutral with regard to jurisdictional claims in published maps and institutional affiliations.



**Copyright:** © 2021 by the authors. Licensee MDPI, Basel, Switzerland. This article is an open access article distributed under the terms and conditions of the Creative Commons Attribution (CC BY) license (<https://creativecommons.org/licenses/by/4.0/>).

## 1. Introduction

Nowadays, one of the major challenges for researchers in chemistry is the elimination of dyestuff from liquid effluents before they are discharged to the external environment in view of their harmful effects on aquatic and terrestrial life [1–4]. This kind of contaminant has characteristics of excellent chemical stability, good solubility in water, high colority and a complex aromatic structure, which decomposition under natural conditions is difficult. The presence of these colorful contaminants in water can restrict light and oxygen getting into water, leading to serious threats to the survival of aquatic organisms. Moreover, most organic dyestuffs, such as azo and anthraquinone dyes, are toxic or carcinogenic to the human body [5–8].

Amongst these dyes, Carmoisine (E 122), also named Azorubine (Az), is used mainly in jams and preserves and was found by the US Certified Color Manufacturers Associ-

ation to be unavoidably contaminated with low levels of beta-naphthylamine, which is well known as a carcinogen [9]. It has also been found to be mutagenic in animal studies [10,11]. For that reason, their removal from effluent containing dye is necessary for our environment protection.

However, the removal of dyes and their products from industrial wastewaters has remained a daunting challenge until now. Various techniques have been used and developed to remove unwanted dyes from contaminated waters, such as photocatalysis, advanced oxidation, electrochemical treatment, precipitation, solvent extraction, reverse osmosis and coagulation/flocculation [12–16]. However, these methods have low efficiencies, high operational energy and produce secondary pollutants [17]. It is therefore of much importance to develop cheap, cost effective and efficient methods to treat these dyes for environmental remediation. Among those, adsorption is a simple, low-cost and effective technique. For this, extensive varieties of adsorbents with higher uptake ability are available to remove the dyes from wastewater, such as SBA-15/graphene oxide nanocomposites, functionalized SBA-15 [18,19] and ceramic membrane [20]. In addition, many nanomaterials with enhanced porosity and higher specific surface area such as MWNTs [19,21,22] and SBA-15/diphenyl carbazon/SDS nanocomposite [19], Zn/Al LDHs intercalated by dodecylsulfate and carbonate using hydrothermal method without calcination [23] have shown also excellent uptake ability. Synthesized starch coated magnetic nanoparticles and polymeric nanocomposites have been also used for the removal of the unspent dyes from the industrial effluents [24]. Moreover, naturally available diatomaceous earth particles surface was modified with mesoporous silica xerogel denotes as diatom xerogel material as well as biosorbent materials have also proved their worth as useful and promising adsorbents to remove the dyes from the industrial effluents [25,26].

Among the various nanomaterials, layered double hydroxides (LDHs) are recognized as hydroxide compounds or anionic clays. They are layered materials containing a metal hydroxide layer with a positive charge intercalated by negatively charged species [27–29]. Their general formula is  $[M^{II}_{1-x}M^{III}_x(OH)_2]^{x+}[A^{n-}_{x/n}mH_2O]$ , where  $M^{2+}$  and  $M^{3+}$  situate in the octahedral holes in a brucite-like layer and  $A^{n-}$  has occupied the hydrated interlayer regions [30]. LDHs have many characteristics such as interlayer anion-exchange capacity, important surface area and surface with a positive charge, which support their application as adsorbents. These properties make them effective adsorbents to uptake organic/inorganic pollutants and principally their negatively charged species [31,32].

In the current work, we report, in the first part, on the successful synthesis of bimetallic (Ni/Zn) hydroxide based bi-structures nanohybrid in mesoporous almost spherical microsystem using simple one-step template-free urea-based hydrothermal technique as high efficiency and low-cost growth process. Afterwards, in the second part, we present their role as an azo dye adsorbent for adsorption application through the detailed investigation of the adsorption process as well as the isotherm models and the kinetics.

## 2. Experimental Procedure

### 2.1. Reagents and Solutions

All the chemicals, urea ( $CH_4N_2O$ , Merck, purity  $\geq 98\%$ ), nickel and zinc chloride (Sigma-Aldrich, purity  $\geq 99.99\%$ ) and Carmoisine dye (di-sodium salt of 2-(4-sulpho-1-naphthylazo)-1-naphthol-4-sulfonic acid ( $C_{20}H_{12}N_2Na_2O_7S_2$ , Merck—Darmstadt, Germany) were of analytical grade and used without further purification.

#### 2.1.1. Adsorbent Ni/Zn Carbonate and/or Hydroxide Based Heterostructure Nanohybrid Synthesis

Nickel (II) chloride hexahydrate ( $NiCl_2 \cdot 6H_2O$ ) (0.1 M) and zinc (II) chloride ( $ZnCl_2$ ) (0.1 M) were dissolved in deionized water at room temperature. Afterwards, 0.5 M urea aqueous solution was added into the above solution and ultrasonicated until a dark green transparent solution was obtained, which was then transferred into a Teflon-lined hydrothermal autoclave system. The latter was sealed, maintained at growth conditions of

180 °C/6 h and then allowed to naturally cool down to room temperature. The obtained green-colored products were filtered and washed with distilled water and ethanol several times before drying in an oven at 80 °C overnight.

### 2.1.2. Adsorbent Characterization Techniques

The synthesized bi-transition metal hydroxide based nanohybrid was characterized using several techniques in order to identify the hydrothermal process product properties, such as structural, textural, morphology and composition, which influence its adsorption performance for environment applications.

Powder X-ray diffraction patterns of our solid adsorbent were collected on an XRD D8 ADVANCE-BRUKER AXS diffractometer equipped with a copper anticathode tube ( $\lambda_{\text{CuK}\alpha} = 1.5406 \text{ \AA}$ ) and a graphite monochromator rear blade, operating at 40 kV–40 mA and employing a scanning rate of  $0.2^\circ \text{ s}^{-1}$  in the range  $10^\circ$ – $90^\circ$ .

Specific contact surface area (SSA) and porosity measurements were carried out using  $\text{N}_2$  adsorption/desorption mechanism at nitrogen liquid temperature (77 K) on a Tristar an ASap2420 sorptometer (Micromeritics) surface area analyzer using Brunauer–Emmett–Teller (BET) and Barrett–Joyner–Halenda (BJH) methods, respectively.

Raman scattering measurement was carried out at room temperature using a Horiba JobinYvon Lab-RAM Aramis confocal Raman spectrometer equipped with a cooled CCD camera and an automated XYZ table at a laser excitation of 532 nm. Using a D2 filter, the estimated laser power that reached the samples was 0.33 mW.

The morphological aspect of this nanohybrid was identified via a field emission scanning electron microscopy FESEM (JEOL 6700-FEG microscope) operated at 3 kV.

Fourier-transform infrared (FTIR) spectra were recorded using a Bruker Vertex 77v spectrometer with a  $4 \text{ cm}^{-1}$  resolution in  $[400\text{--}4000 \text{ cm}^{-1}]$  range controlled with an Opus software analysis.

### 2.1.3. Analytical Method

A calibration curve was prepared using the standard solutions of Az with different concentrations from 0.5 to  $50 \text{ mg L}^{-1}$ . The efficiency of the proposed process was evaluated by monitoring Az removal after measuring the absorbance at  $\lambda_{\text{max}} = 519 \text{ nm}$ .

The azo dye adsorption capacity  $q_t$  ( $\text{mg g}^{-1}$ ) and the removal ratio  $R$  (%) were obtained from the following relations:

$$q_t = (C_0 - C_t) \frac{V}{W} \quad (1)$$

$$R (\%) = \frac{(C_0 - C_t)}{C_0} * 100 \quad (2)$$

where  $C_0$  and  $C_t$  are the initial and the equilibrium concentration of Az in the solution ( $\text{mg L}^{-1}$ ), where  $W$  the adsorbent dry weight (g) and  $V$  is the suspension volume (l).

## 3. Adsorption Studies

### 3.1. Batch Adsorption

Batch adsorption tests were carried out at a constant temperature using a water bath. The initial concentration of Azorubine solution was  $50 \text{ mg L}^{-1}$  for all experiments, except for those carried out to determine the effect of the initial dye concentration. The adsorbent was put in selected flask of 100 mL dye solution and vigorously stirred at 25 °C, except experiments of the temperature effect. The experiments were conducted at natural pH of mixtures without further adjustment, except also for the step of solution pH effect where it was adjusted using (0.1 N) HCl or NaOH in separate experiments. Batch studies were performed as function of the adsorbent rate ranging from (0.01 to 0.05 g), pH solution from 2 to 12 and adsorbate concentrations from 20 to  $200 \text{ mg L}^{-1}$ .

### 3.2. Isotherm Models

The adsorption isotherm was used to represent the adsorption capacity at different solution concentrations that helps to have idea on the adsorbent and adsorbate interaction. The experimental results were fitted using Langmuir [33] and Freundlich [34] models. The Langmuir isotherm (Equation (3)) assumes a monolayer adsorption of the adsorbate on the adsorbent surface using a given relation:

$$\frac{1}{q_e} = \frac{1}{q_m} + \frac{1}{K_L \cdot q_m} + \frac{1}{C_e} \quad (3)$$

where  $q_m$  is the maximum adsorption capacity ( $\text{mg g}^{-1}$ ) and  $K_L$  is the Langmuir constant ( $\text{L mg}^{-1}$ ).

Nevertheless, the Freundlich adsorption isotherm (Equation(4)) as an empirical equation often used to describe the chemisorption on heterogeneous surface is given by the following relation:

$$\text{Ln } q_e = \text{Ln } K_F + \frac{1}{n} \text{Ln } C_e \quad (4)$$

where  $K_F$  is the Freundlich constant and  $1/n$  is the heterogeneity factor. In this Freundlich equation,  $1/n$  values between 0 and 1 indicate that the adsorption is favorable.

### 3.3. Kinetic Studies

The pseudo-first-order and pseudo-second-order kinetic models are described as following [35]:

$$\text{Ln } (q_e - q_t) = \text{Ln } q_e - K_1 t \quad (5)$$

$$\frac{t}{q_e} = \frac{1}{q_e} t + \frac{1}{K_2 q_e^2} \quad (6)$$

where  $q_e$  ( $\text{mg g}^{-1}$ ) is the equilibrium adsorption capacity,  $q_t$  ( $\text{mg g}^{-1}$ ) is the adsorption capacity at time  $t$ ;  $k_1$  ( $\text{min}^{-1}$ ) is the rate constant of the first-order adsorption and  $k_2$  ( $\text{g} \cdot \text{mg}^{-1} \text{min}^{-1}$ ) is the rate constant of the second-order adsorption.

## 4. Results and Discussion

### 4.1. Characterization of Adsorbent

The description of the XRD pattern and FTIR spectrum of the as-synthesized Ni/Zn based nanostructure which will be used as adsorbent in this investigation are presented in Figure 1. Figure 1a shows the formation of bi-nanostructures based on nickel hydrate hydroxide ( $\alpha\text{-Ni}(\text{OH})_2 \cdot 0.75\text{H}_2\text{O}$ ) and zinc carbonate hydroxide ( $\text{Zn}_5(\text{CO}_3)_2(\text{OH})_6$ ) which are assigned to rhombohedral [JCPDS no. 038-0715] and monoclinic [JCPDS no. 19-1458] structure, respectively, with 54% crystallinity order.

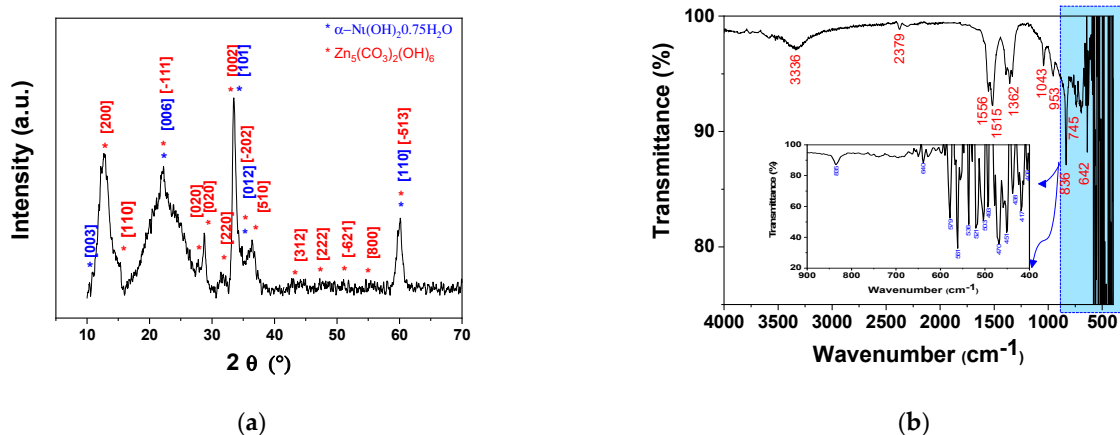


**Figure 1.** Adsorbent based on Ni/Zn LDH bi-nanostructure nanostructure synthesized via hydrothermal process at 6h/180  $^\circ\text{C}$ : XRD diffractogram (a) and FTIR spectrum (b).

Table 1 summarizes the bi-phase nanohybrid structural characteristics depending on their diffractogram.

**Table 1.** Structural characteristics of Ni/Zn based bi-phase nanohybrid.

Phase	a (Å)	b (Å)	c (Å)
Zn <sub>5</sub> (CO <sub>3</sub> ) <sub>2</sub> (OH) <sub>6</sub>	13.83	6.19	5.386
Ref. [JCPDS no.19 1458]	13.58	6.28	5.41
α-Ni(OH) <sub>2</sub> ·0.75H <sub>2</sub> O	3.06	-	24
Ref. [JCPDS no.038-0715]	3.08	-	23.41

The FTIR spectrum of this nanoadsorbent as shown in Figure 1b is typical of a hydrotalcite-like material showing a broad and intense band at 3336 cm<sup>-1</sup> that can be attributed to hydroxyl (OH<sup>-</sup>) stretching vibrations from structural hydroxyl groups and interlayer water molecules [36]. In addition, bands at 1362 cm<sup>-1</sup> (ν<sub>3</sub>), 1043 cm<sup>-1</sup> (ν<sub>1</sub>) and 745 cm<sup>-1</sup> (ν<sub>2</sub>) [37] show the presence of carbonate anion (CO<sub>3</sub><sup>2-</sup>) in the interlayer [38]. However, the bands at 953 and 836 cm<sup>-1</sup> are associated with metal–oxygen (M–O) and metal–hydroxyl (M–OH) groups in the lattice of LDHs. More precisely, below 642 cm<sup>-1</sup>, the recorded bands are attributed to δ Ni/Zn–OH or ν Ni/Zn–O as reported in many studies [39–41]. Moreover, the sharp band at 836 cm<sup>-1</sup> is associated with in-plane quadrant bending [39–41]. These results clearly prove the XRD identification reported above.

The morphological and textural properties of this Ni/Zn based LDH nanohybrid illustrate that it possesses precisely special membranous morphology with non-homogeneous mesopores in an agglomerated way as shown in Figure 2a.

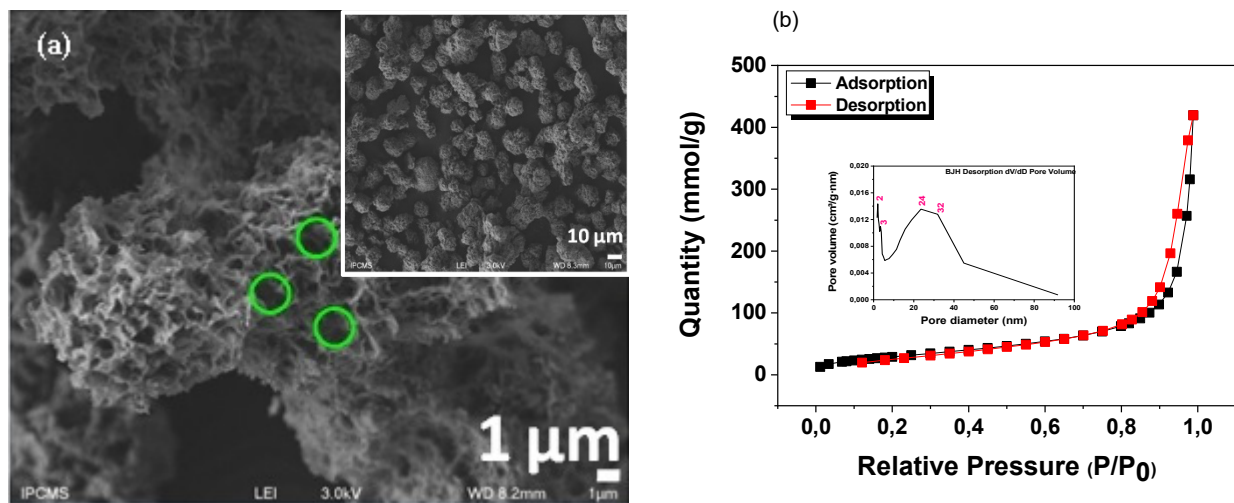


**Figure 2.** FESEM micrographs (a) and their N<sub>2</sub> adsorption-desorption isotherms (inset pore distribution) (b) of adsorbent based on Ni/Zn bi-phase nanohybrid.

The specific surface area (SSA—S<sub>BET</sub>) of this bi-phase nanohybrid was estimated from the adsorbed-desorbed nitrogen quantity in relation to its pressure at liquid boiling point and under normal atmospheric pressure. Figure 2b shows the obtained information of adsorption and desorption isotherms of nitrogen at 77 K and their pore size and volume distribution according to the BET and BJH model, respectively. The isotherm shows an hysteresis IV-type with S<sub>BET</sub> of about 110.38 m<sup>2</sup> g<sup>-1</sup>. However, the pore size distribution illustrated in the inset of this figure indicates the collection of multiporous nanohybrid with average pore size essentially centered at 2, 3, 24 and 32 nm, which demonstrates their mesoporous texture nanohybrid (pores between 2 and 50 nm) [42]. This distribution confirms, again, the dishomogeneous porous morphology observed in almost micro/nanospheric membranous architecture via FESEM microscopy as shown above.

To better understand the composition of the used nanohybrid based adsorbent as well as the existing functional groups that act on the adsorption mechanism, XPS analysis was performed. Figure 3 shows the deconvolution of main asymmetric peaks ( $\text{Ni}_{2p}$ ,  $\text{Zn}_{2p}$ ,  $\text{C}_{1s}$ , and  $\text{O}_{1s}$ ) of high-resolution core-level XPS spectra, using L/G fitting method consistent with the literature data [36,43].  $\text{Ni}_{2p}$  and  $\text{Zn}_{2p}$  show that the oxidation state of these elements is mainly based on ions, namely  $\text{Ni}^{2+}$  (or  $\text{Zn}^{2+}$ ) as in previously reported data, which will be very beneficial in our adsorption process [36,44].

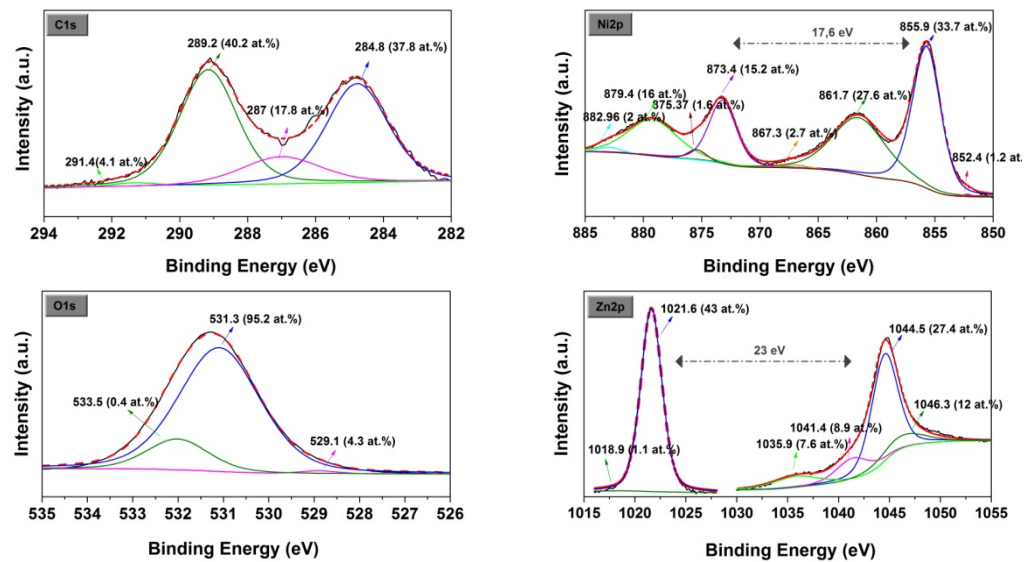


Figure 3. XPS spectra of the Ni/Zn LDH-based adsorbent in the  $\text{Ni}_{2p}$ ,  $\text{Zn}_{2p}$ ,  $\text{C}_{1s}$ ,  $\text{O}_{1s}$  energy regions.

## 4.2. Adsorption Process from Aqueous Solutions

### 4.2.1. Adsorbent Dosage Effect on the Azorubine Removal

One of the parameters that significantly affect the adsorption capacity is the adsorbent dosage [45]; Figure 4 illustrates the Ni/Zn LDH dosage effect on Az adsorption. The removal ratio of azo dye was increased when increasing the amount of Ni/Zn LDH adsorbent that was used. High Az removal is observed, with the maximum reaching a value of 97% with  $30 \text{ mg L}^{-1}$  adsorbent. This can be attributed to the larger pore diameter (around 24 nm), which favors Az removal at lower adsorbent dosages [45]. In addition, the higher sorbent removal with Ni/Zn LDHs at low adsorbent dosage demonstrates the high affinity between this adsorbent and the Az. Therefore, we fixed the adsorbent amount to  $30 \text{ mg L}^{-1}$  for all subsequent experiments.

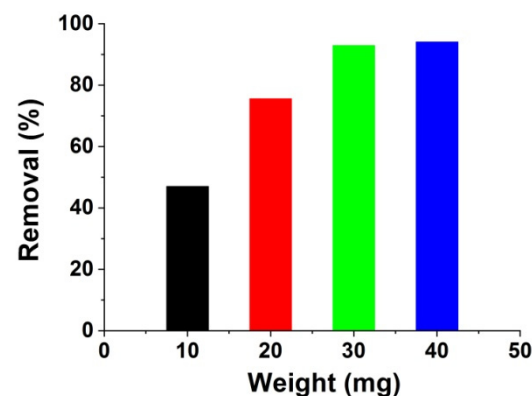
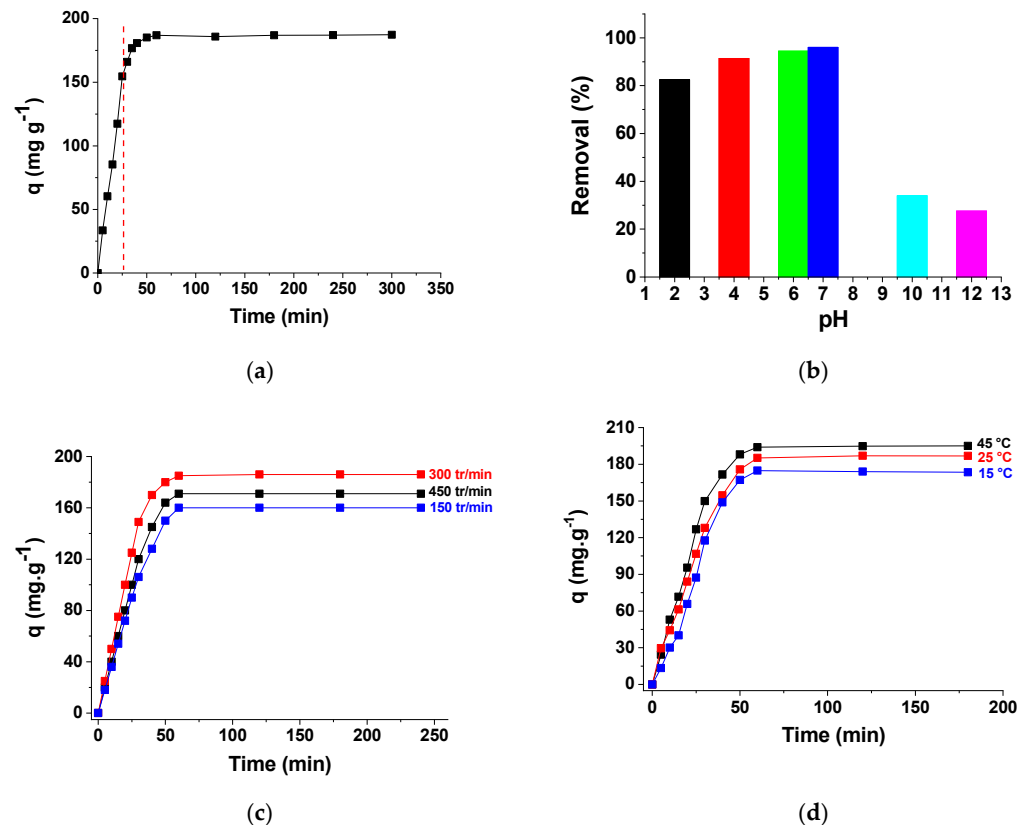


Figure 4. Ni/Zn LDH adsorbent dosage effect on Carmoisine (Az) removal.

#### 4.2.2. Contact Time, pH, Stirring Speed and Temperature Effect on the Adsorption Process

The adsorption as a function of contact time was conducted at room temperature (25 °C) using 30 mg L<sup>-1</sup> of Ni/Zn LDH and is reported in Figure 5a. The azo dye uptake was rather fast initially (first 25 min), then increased slowly up until 60 min, when the equilibrium was reached with a removal ratio of 94.3%. At the beginning, there are phenomena attributed to the existence of a large number of vacant active sites on the adsorbent surface. However, the remaining vacant surface sites are less available for adsorption with time probably due to the repulsive forces that occur between the Az molecules and the Ni/Zn LDH surfaces [46].



**Figure 5.** Contact time (a), pH (b) and stirring speed (c) effect on the Carmoisine (Az) removal using Ni/Zn LDH adsorbent (initial dye concentration = 50 mg L<sup>-1</sup> in 100 mL; sorbent mass = 30 mg; T = 25 °C; initial pH). (d) Kinetics of Az uptake by nanoadsorbents at various temperature (initial dye concentration = 50 mg L<sup>-1</sup> in 100 mL; sorbent mass = 30 mg; stirring speed = 300 rpm; initial pH).

Otherwise, the decrease in the Az adsorption kinetics is due to the presence of carbonates from LDH structure; the dye species are in competition with carbonate anions which originate from strong interactions between the CO<sub>2</sub> molecules and the strongest basic sites in the LDH structure and, consequently, it takes more time to reach the adsorption equilibrium [47].

The pH of the dye solution is also an important parameter which controls the rate of synthetic azo dye solution degradation. In order to study this pH effect, the degradation experiments were carried out using 30 mg of Ni/Zn hydroxide in a solution of 50 ppm Az (Figure 5b) by varying the pH in the range 2–12 with addition of (0.1 M) either HCl or NaOH. The adsorption process affected by the milieu pH is possibly due to the interactions between the dye anions in the solution and the adsorbent surface charge contents [48,49]. Therefore, we noted firstly that the removal efficiency of Az increases from 82.52% to 96.02% when the pH is varied from 2 to 7, and the maximum was achieved at neutral pH.

Then, the removal rate decreases in basic environment from 33.96% to 27.54% in the pH range from 10 to 12. This phenomenon can be attributed to the electrostatic attraction

between the positively charged adsorbent surface layer and the anionic dye at pH less than the point of zero charge (PZC), which is equal to 7.53 for our Ni/Zn LDH adsorbent. Therefore, at lower pH (acidic region), the surface of Ni/Zn LDH adsorbent with more positively charged ( $\text{pH} < \text{pH}_{\text{PZC}}$ ) leads to increase the percentage of dye removal due to strengthening the attractive forces among the positive charge of the surface of the LDHs and negative charge of the dye [50]. On the other hand, the surface of LDHs become more negatively charged along with the increase in solution pH ( $\text{pH} > \text{pH}_{\text{PZC}}$ ), leading to a decline in the nano-hybrid adsorption ability. This decrease phenomenon is related to strong repulsion forces between the dye and negative surface of the LDHs containing inorganic anions. Consequently, for pH values under the  $\text{pH}_{\text{PZC}}$ , there can be two probable mechanisms to propose for Az removed using this kind of LDH; the first mechanism could concern the anionic exchange of carbonate anions in the interlayer with dye anions  $\text{Az-SO}_3^-$ , while the second is the fixation by adsorption with the positively charged surface  $\text{H}_2\text{O}^+$  of Ni/Zn LDH and the Az anions [23]. Therefore, these solutions were used directly without any pH adjustment in the rest of the work.

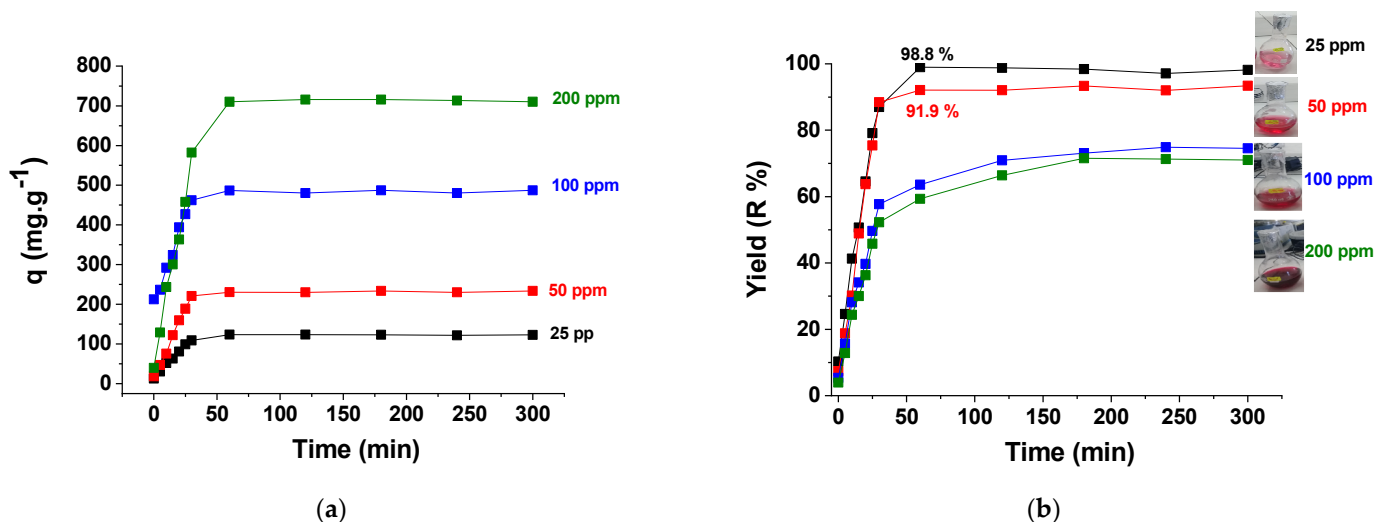
According to the curves in Figure 5c, it can be seen that the capacity for retention of the dye increases slightly with increasing stirring speed, which acts favorably on the contact probability between substrate and support.

Figure 5d presents Az removal as a function of time at three different temperatures (15, 25 and 45 °C) on Ni/Zn LDH adsorbent. A similar profile of the kinetic curves is observed for the three temperatures, and the sorption kinetic increases slightly with increasing temperature.

This indicates that the sorption process is endothermic. The phenomenon could be ascribed to the improvement of the mobility and the penetration of Az molecules within the Ni/Zn LDH based mesoporous bi-nanostructure by allowing the activation energy barrier to be easily overcome [51].

#### 4.2.3. Adsorbent Concentration Effect on the Adsorption Process

Figure 6 exhibits the adsorption capacity of the Ni/Zn LDH nano-hybrid at various initial concentrations of Az. It can be seen that the removal percentage decreases from 98% to 66.8% and the Az adsorption amount increases from 123.74 to 710  $\text{mg g}^{-1}$  when the Az initial concentration is increased from 25 to 200  $\text{mg L}^{-1}$ . Therefore, the decrease in the dye removal efficiency with an increase in the dye concentration may be related to the initial amount of dye molecules (see pictures inset), which is lower than the available surface active sites, making the adsorption ratio independent of the initial dye concentration. Nevertheless, at higher concentrations, there would be fewer available sites than initial dye molecules in the solution which affect the Az removal percentage [46,52].



**Figure 6.** Effect of the initial Az concentration on (a) the adsorption capacity of Ni/Zn LDH adsorbent and (b) the Az removal ratio.

Moreover, our nanoadsorbent has a high elimination rate just in the first few minutes, and the adsorption equilibrium time was 60 min. It shows that the adsorption on Ni/Zn LDH nano hybrid as a micro/nanoporous system has a short equilibrium time, and the adsorption rate of this nano hybrid is much faster than other general bulk layered compound. This can be attributed to the mesoporous micro/nanosystem morphology, which is helpful for molecular transport by virtue of its porous texture architectural feature [53–56].

#### 4.3. Fitting Kinetic Models

The kinetic curves of Az adsorption onto Ni/Zn LDH nano hybrid are shown in Figure 7a,b, and the parameters of these kinetics models were obtained by regression analysis and listed in Table 2. We observed that the  $R^2$  coefficients determined for the pseudo-first-order model were higher than the pseudo-second-order model values for this nano hybrid adsorbent.

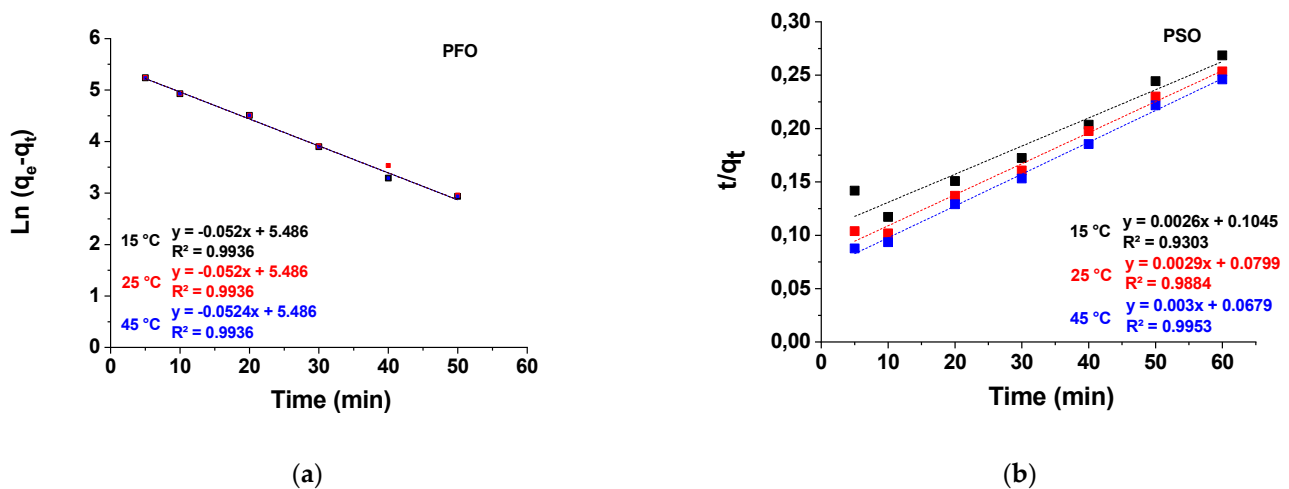


**Figure 7.** Adsorption kinetics of Az on Ni/Zn LDH nano hybrid: (a) pseudo-first-order, (b) pseudo-second-order (PSO) kinetics model.

**Table 2.** Coefficients of pseudo-first-order (PFO) and pseudo-second-order (PSO) adsorption kinetic models.

Models	Characteristics	Temperature K		
		288.15 K	298.15 K	318.15 K
Pseudo-first-order (PFO) model	$q_{e-exp}$ [ $\text{mg g}^{-1}$ ]	223.44	236.74	243.94
	$k_1$ [ $\text{min}^{-1}$ ]	0.0524	0.0523	0.0523
	$q_{e-cal}$ [ $\text{mg g}^{-1}$ ]	241.29	240.44	240.44
	$R^2$	0.9949	0.9949	0.9949
Pseudo-second-order (PSO) model	$k_2$ [ $\text{min}^{-1}$ ]	09.57	12.51	14.72
	$q_{e-cal}$ [ $\text{mg g}^{-1}$ ]	384.61	344.83	333.33
	$R^2$	0.9419	0.9903	0.9961

In addition, the computed equilibrium uptakes of the pseudo-first-order (PFO) expression are closer to the experimental values, thus indicating the applicability of this model, which can describe very well the Az sorption process onto Ni/Zn LDH nano adsorbent via a physical sorption [57].

#### 4.4. Adsorption Isotherm Studies

In general, adsorption isotherms play a fundamental role in the optimization of adsorbent consumption and explains the reaction between the pollutants and the adsorbent material [58]. Hence, the choice of best isotherm fit was conducted by linear regression analyses and a comparison of their correlation coefficients ( $R^2$ ).

Equilibrium studies which express the dye adsorbent capacity are explained through the adsorption isotherms. The kinetic curves of Az adsorption onto Ni/Zn LDH nano-hybrid are shown in Figure 8, and their parameters were obtained by regression analysis and listed in Table 3.

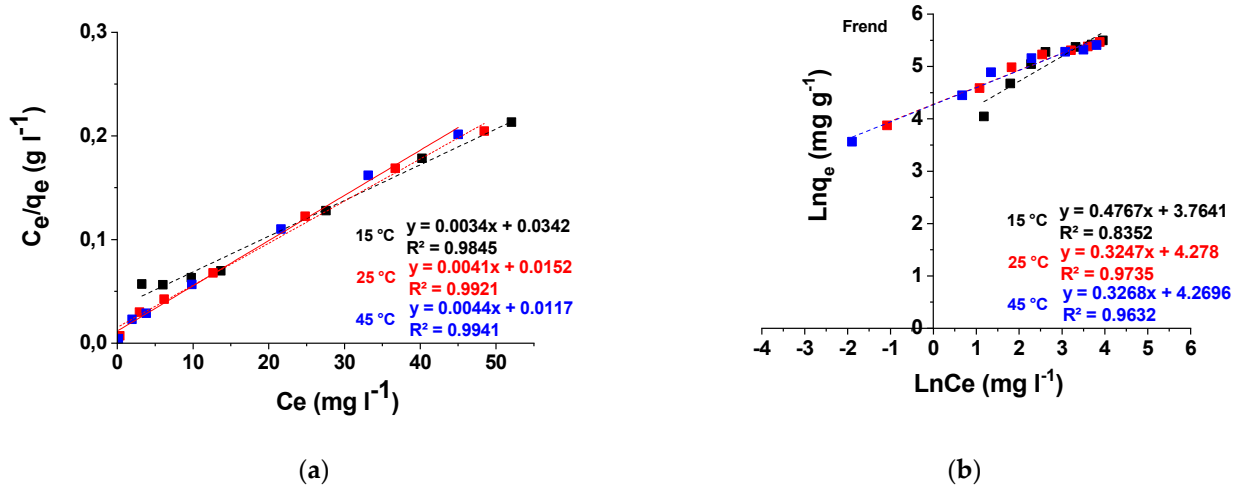


**Figure 8.** Adsorption isotherms of Az dye on Ni/Zn LDH nano-hybrid for two models: (a) Langmuir and (b) Freundlich model.

**Table 3.** Langmuir and Freundlich constants for Az adsorption onto Ni/Zn LDH nano-hybrid.

Models	Isotherm Constants	Temperature K		
		288 K	298 K	318 K
Langmuir	$q_{e\text{-exp}}$ [mg g <sup>-1</sup> ]	223.44	236.74	243.94
	$R^2$	0.9952	0.9934	0.9871
	$K_L$ [l mg <sup>-1</sup> ]	0.376	0.270	0.099
	$Q_{\text{max}}$ [mg g <sup>-1</sup> ]	227.273	243.902	294.118
	$R_L$	0.050	0.069	0.167
Freundlich	$R^2$	0.9694	0.9779	0.8626
	$K_F$ (mg g <sup>-1</sup> )	71.58	72.35	43.12
	$N$	3.128	3.123	2.097

The values of the correlation coefficient  $R^2 = 0.9952$ ,  $0.9934$  and  $0.9871$  at 288, 298 and 318 K, respectively, of the Az adsorption process on our nano-hybrid, demonstrate good linearity with the Langmuir expression compared to the Freundlich model. This result reveals the monolayer coverage of Az molecules on the NiZn/LDH nano-hybrid accompanied by a homogeneous adsorption process. Moreover, the equilibrium parameter  $R_L$  ( $\frac{1}{1+bC_0}$ ) is in the range of [0–1], indicating that implying the Az adsorption process is favorable. Moreover, the higher values of  $K_F$  (71.58, 72.35 and 43.12 mg g<sup>-1</sup>) and  $N$  (3.128, 3.123 and 2.097) at 288, 298 and 318 K temperatures, respectively, indicate that this Ni/Zn LDH nano-hybrid has a higher adsorption capacity and affinity for the azo dye molecules, revealing the favorability of this adsorption [59].

Moreover, the theoretical maximum adsorption capacity of Ni/Zn LDH mesoporous nano-adsorbent calculated depending on the Langmuir model is 227.27 mg g<sup>-1</sup>, which is four times more superior than that of other analogical or low-cost adsorbents such as the 3D magnetic hollow porous Ni-ferrites (3D-MHP-NiFe<sub>2</sub>O<sub>4</sub>) with  $q_m = 53.13$  mg g<sup>-1</sup> [60] and copper oxide with  $q_m = 1.59$  mg g<sup>-1</sup> [59].

## 5. Conclusions

In summary, Ni/Zn layered double hydroxide based nano-hybrid was obtained using low-cost template-free hydrothermal process at 180 °C growth temperature during 6 h via

the formation of two phases based of nickel hydrate hydroxide ( $\alpha^*-\text{Ni}(\text{OH})_2 \cdot 0.75 \text{H}_2\text{O}$ ) and zinc carbonate ( $\text{Zn}_5(\text{CO}_3)_2 (\text{OH})_6$ ), where the FTIR results also indicate the presence of functional groups that favor their electrostatic attraction with the anionic dye.

This multiscale porous hydroxide based nanohybrid with irregular-like nanoflakes in 3D spongy shape hierarchical micro/nanostructures which possess very interesting specific surface area around  $110 \text{ m}^2 \text{ g}^{-1}$  with reasonable pore volume and pore size distribution between  $[0.16\text{--}0.85 \text{ cm}^3 \text{ g}^{-1}]$  and  $[12\text{--}32 \text{ nm}]$ , respectively, is accompanied by mixed oxidation states with two kinds of anions  $\text{Ni}^{2+}$  (or  $\text{Zn}^{2+}$ ) and  $\text{Ni}^{3+}$  (or  $\text{Zn}^{3+}$ ), allowing it to be a very good nanoadsorbent.

The Az adsorption ability of this new kind of nanoadsorbent was systematically investigated using kinetic and equilibrium studies as well as by examining the effect of dosage adsorbents, initial adsorbate concentration, initial pH, temperature, etc. Thus, the capacity sorption of Az increases with increasing Az concentration, with a very fast sorption process whereby an equilibrium time of 60 min was obtained. The adsorption behavior of dye onto this Ni/Zn LDH nanohybrid was obviously influenced by the pH with the best removal efficiency at pH range from 6 to 7. We also, noted that our new nanoadsorbent presents an important adsorption capacity ( $\sim 223 \text{ mg g}^{-1}$ ) compared to other materials. Moreover, the sorption kinetic data were more suitable with the pseudo-first-order (PFO) kinetic model. Langmuir adsorption isotherm model showed the best compatibility with the experimental data in comparison with other isotherm models.

**Author Contributions:** Conceptualization, A.N.-M. and O.G.; methodology, A.N.-M.; validation, A.N.-M. and O.G.; investigation, A.N.-M. and O.G.; resources, S.D. and N.H.; writing—original draft preparation, A.N.-M. and O.G.; writing—review and editing, A.N.-M. and O.G.; supervision, A.H. and M.G.; Samples analysis, D.B. and J.E.-H. All authors have read and agreed to the published version of the manuscript.

**Funding:** This research received no external funding.

**Institutional Review Board Statement:** Not applicable.

**Informed Consent Statement:** Informed consent was obtained from all subjects involved in the study.

**Data Availability Statement:** Not applicable.

**Acknowledgments:** The present work is based on the research carried out at LEREC laboratory, Badji Mokhtar-Annaba University under Directorate General for Scientific Research and Technological Development (DGRSDT)—Algeria. We are also very grateful to J. El-Haskouri from Valencia polytech—Spain for his help to complete characterizations (XPS and BET analysis). This research did not receive any specific grant from funding agencies in the public, commercial, or not-for-profit sectors.

**Conflicts of Interest:** The authors declare no conflict of interest.

## References

1. Atun, G.; Ayar, N.; Kurtoğlu, A.E.; Ortoboy, S. A comparison of sorptive removal of anthraquinone and azo dyes using fly ash from single and binary solutions. *J. Hazard. Mater.* **2019**, *371*, 94–107. [[CrossRef](#)]
2. Hayat, A.; Catanante, G.; Marty, J.L. Current Trends in Nanomaterial-Based Amperometric Biosensors. *Sensors* **2014**, *14*, 23439–23461. [[CrossRef](#)] [[PubMed](#)]
3. Rocha, O.P.; Cesila, C.A.; Christovam, E.M.; de Barros, S.B.M.; Zaroni, M.V.B.; de Oliveira, D.P. Ecotoxicological risk assessment of the “Acid Black 210” dye. *Toxicology* **2017**, *376*, 113–119. [[CrossRef](#)]
4. Tan, K.B.; Vakili, M.; Horri, B.A.; Poh, P.E.; Abdullah, A.Z.; Salamatinia, B. Adsorption of dyes by nanomaterials: Recent developments and adsorption mechanisms. *Sep. Purif. Technol.* **2015**, *150*, 229–242. [[CrossRef](#)]
5. Huang, Q.; Song, S.; Chen, Z.; Hu, B.; Chen, J.; Wang, X. Biochar-based materials and their applications in removal of organic contaminants from wastewater: State-of-the-art review. *Biochar* **2019**, *1*, 45–73. [[CrossRef](#)]
6. Huang, Q.; Liu, M.; Wan, Q.; Jiang, R.; Mao, L.; Zeng, G.; Huang, H.; Deng, F.; Zhang, X.; Wei, Y. Preparation of polymeric silica composites through polydopamine-mediated surface initiated ATRP for highly efficient removal of environmental pollutants. *Mater. Chem. Phys.* **2017**, *193*, 501–511. [[CrossRef](#)]
7. Mahmood, S.; Khalid, A.; Arshad, M.; Mahmood, T.; Crowley, D.E. Detoxification of azo dyes by bacterial oxidoreductase enzymes. *Crit. Rev. Biotechnol.* **2015**, *36*, 639–651. [[CrossRef](#)] [[PubMed](#)]

8. Donadelli, J.A.; Carlos, L.; Arques, A.; Einschlag, F.S.G. Kinetic and mechanistic analysis of azo dyes decolorization by ZVI-assisted Fenton systems: pH-dependent shift in the contributions of reductive and oxidative transformation pathways. *Appl. Catal. B Environ.* **2018**, *231*, 51–61. [[CrossRef](#)]
9. Tuormaa, T.E. The Adverse Effects of Food Additives on Health: A Review of the Literature with Special Emphasis on Childhood Hyperactivity. *J. Orthomol. Med.* **1994**, *9*, 225–243.
10. Biswas, M.M.; Taylor, K.E.; Bewtra, J.K.; Biswas, N. Enzymatic treatment of sulfonated aromatic amines generated from reductive degradation of reactive azo dyes. *Water Environ. Res.* **2007**, *79*, 351–356. [[CrossRef](#)] [[PubMed](#)]
11. Venkata Mohan, S.; Chandrasekhar Rao, N.; Karthikeyan, J. Adsorptive removal of direct azo dye from aqueous phase onto coal based sorbents: A kinetic and mechanistic study. *J. Hazard. Mater. B* **2002**, *90*, 189–204. [[CrossRef](#)]
12. Ali, N.; Awais, K.T.; Ul-Islam, M.; Khan, A.; Shah, S.J.; Zada, A. Chitosan-coated cotton cloth supported copper nanoparticles for toxic dye reduction. *Int. J. Biol. Macromol.* **2018**, *111*, 832–838. [[CrossRef](#)] [[PubMed](#)]
13. Zada, A.; Qu, Y.; Ali, S.; Sun, N.; Lu, H.; Yan, R.; Zhang, X.; Jing, L. Improved visible-light activities for degrading pollutants on TiO<sub>2</sub>/g-C<sub>3</sub>N<sub>4</sub> nanocomposites by decorating SPR Au nanoparticles and 2,4-dichlorophenol decomposition path. *J. Hazard. Mater.* **2018**, *342*, 715–723. [[CrossRef](#)]
14. Hisada, M.; Tomizawa, Y.; Kawase, Y. Removal kinetics of cationic azo-dye from aqueous solution by poly- $\gamma$ - glutamic acid biosorbent: Contributions of adsorption and complexation / precipitation to Basic Orange 2 removal. *J. Environ. Chem. Eng.* **2019**, *7*, 103157. [[CrossRef](#)]
15. Kang, Y.; Yoon, H.; Lee, C.; Kim, E.; Chang, Y. Advanced oxidation and adsorptive bubble separation of dyes using MnO<sub>2</sub>-coated Fe<sub>3</sub>O<sub>4</sub> nanocomposite. *Water Res.* **2019**, *151*, 413–422. [[CrossRef](#)]
16. Nazir, R.; Khan, M.; Rehman, R.U.; Shujah, S.; Khan, M.; Ullah, M.; Zada, A.; Mahmood, N.; Ahmad, I. Adsorption of selected azo dyes from an aqueous solution by activated carbon derived from *Monotheca buxifolia* waste seeds. *Soil Water Res.* **2020**, *15*, 166–172. [[CrossRef](#)]
17. Ullah, M.; Nazir, R.; Khan, M.; Khan, W.; Shah, M.; Afridi, S.G.; Zada, A. The effective removal of heavy metals from water by activated carbon adsorbents of *Albizia lebbek* and *Melia azedarach* seed shells. *Soil Water Res.* **2020**, *15*, 30–37. [[CrossRef](#)]
18. Mirabi, A.; Rad, A.S.; Divsalar, F.; Karimi-Maleh, H. Application of SBA-15/Diphenyl Carbazon/SDS Nanocomposite as Solid-Phase Extractor for Simultaneous Determination of Cu(II) and Zn(II) Ions. *Arab. J. Sci. Eng.* **2018**, *43*, 3547–3556. [[CrossRef](#)]
19. Mirabi, A.; Rad, A.S.; Abdollahi, M. Preparation of modified MWCNT with dithiooxamide for preconcentration and determination of trace amounts of cobalt ions in food and natural water samples. *ChemistrySelect* **2017**, *2*, 4439–4444. [[CrossRef](#)]
20. Ahmad, R.; Guo, J.; Kim, J. Structural characteristics of hazardous organic dyes and relationship between membrane fouling and organic removal efficiency in fluidized ceramic membrane reactor. *J. Clean. Prod.* **2019**, *232*, 608–616. [[CrossRef](#)]
21. Shabaan, O.A.; Jahin, H.S.; Mohamed, G.G. Removal of anionic and cationic dyes from wastewater by adsorption using multiwall carbon nanotubes. *Arab. J. Chem.* **2020**, *13*, 4797–4810. [[CrossRef](#)]
22. Nait-Merzoug, A.; Guellati, O.; Benjaballah, A.; Janowska, I.; Bégin, D.; Manyala, N.; Guerioune, M. Tartrazine removal from water using functionalized multiwall carbon nanotubes. *Desalin. Water Treat.* **2017**, *67*, 397–405. [[CrossRef](#)]
23. Mahjoubi, F.Z.; Khalidi, A.; Elhalil, A.; Barka, N. Characteristics and mechanisms of methyl orange sorption onto Zn/Al layered double hydroxide intercalated by dodecyl sulfate anion. *Sci. Afr.* **2019**, *6*, e00216. [[CrossRef](#)]
24. Stan, M.; Lung, I.; Soran, M.L.; Opris, O.; Leostean, C.; Popa, A.; Copaciu, F.; Lazar, M.D.; Kacso, I.; Silipas, T.D.; et al. Starch-coated green synthesized magnetite nanoparticles for removal of textile dye Optilan Blue from aqueous media. *J. Taiwan Inst. Chem. Eng.* **2019**, *100*, 65–73. [[CrossRef](#)]
25. Deniz, F. Bioremediation potential of waste biomaterials originating from coastal *Zostera marina* L. meadows for polluted aqueous media with industrial effluents. *Prog. Biophys. Mol. Biol.* **2019**, *145*, 78–84. [[CrossRef](#)]
26. Ganesan, S.; Bhat, M.P.; Kigga, M.; Uthappa, U.T.; Jung, H.Y.; Kumeria, T.; Kurkuri, M.D. Amine activated diatom xerogel hybrid material for efficient removal of hazardous dye. *Mater. Chem. Phys.* **2019**, *235*, 121738. [[CrossRef](#)]
27. Mohapatra, L.; Parida, K. A review on the recent progress, challenges and perspective of layered double hydroxides as promising photocatalysts. *J. Mater. Chem. A* **2016**, *4*, 10744–10766. [[CrossRef](#)]
28. Arrabito, G.; Bonasera, A.; Prestopino, G.; Orsini, A.; Mattoccia, A.; Martinelli, E.; Pignataro, B.; Medaglia, P.G. Layered double hydroxides: A Toolbox for Chemistry and Biology. *Crystals* **2019**, *9*, 361. [[CrossRef](#)]
29. Mishra, G.; Dash, B.; Pandey, S. Layered double hydroxides: A brief review from fundamentals to application as evolving biomaterials. *Appl. Clay Sci.* **2018**, *153*, 172–186. [[CrossRef](#)]
30. Elhalil, A.; Qourzal, S.; Mahjoubi, F.Z.; Elmoubarki, R.; Farnane, M.; Tounsadi, H.; Sadiq, M.; Abdennouri, M.; Barka, N. Defluoridation of groundwater by calcined Mg/Al layered double hydroxide. *Emerg. Contam.* **2016**, *2*, 42–48. [[CrossRef](#)]
31. Ai, L.; Zhang, C.; Meng, L. Adsorption of Methyl Orange from Aqueous Solution on Hydrothermal Synthesized Mg-Al Layered Double Hydroxide. *J. Chem. Eng. Data* **2011**, *56*, 4217–4225. [[CrossRef](#)]
32. Qu, J.; He, X.; Li, X.; Ai, Z.; Li, Y.; Zhang, Q.; Liu, X. Precursor preparation of Zn-Al layered double hydroxide by ball milling for enhancing adsorption and photocatalytic decoloration of methyl orange. *RSC Adv.* **2017**, *7*, 31466–31474. [[CrossRef](#)]
33. Langmuir, I. The adsorption of gases on plane surfaces of glass, mica and platinum. Contribution from the research laboratory of the general electric Co. *J. Am. Chem. Soc.* **1918**, *40*, 1361–1403. [[CrossRef](#)]
34. Lacin, D.; Aroguz, A.Z. Kinetic studies on adsorption behavior of methyl orange using modified halloysite, as an eco-friendly adsorbent. *SN Appl. Sci.* **2020**, *2*, 2091. [[CrossRef](#)]

35. Mittal, A.; Mittal, J.; Malviya, A.; Kaur, D.; Gupta, V.K. Adsorption of hazardous dye crystal violet from wastewater by waste materials. *J. Colloid Interface Sci.* **2010**, *343*, 463–473. [[CrossRef](#)]
36. Habib, N.; Guellati, O.; Harat, A.; Nait-Merzoug, A.; El Haskouri, J.; Momodu, D.; Manyala, N.; Begin, D.; Guerioune, M. Ni–Zn hydroxide-based bi-phase multiscale porous nanohybrids: Physico-chemical properties. *Appl. Nanosci.* **2020**, *10*, 2467–2477. [[CrossRef](#)]
37. Wang, X.; Hu, J.; Liu, W.; Wang, G.; An, J.; Lian, J. Ni/Zn binary system hydroxide, oxide and sulfide materials: Synthesis and high supercapacitor performance. *J. Mater. Chem. A* **2015**, *3*, 23333–23344. [[CrossRef](#)]
38. Luengo, C.V.; Volpe, M.A.; Avena, M.J. High sorption of phosphate on Mg–Al layered double hydroxides: Kinetics and equilibrium. *J. Environ. Chem. Eng.* **2017**, *5*, 4656–4662. [[CrossRef](#)]
39. Buazar, F.; Baghlani-Nejzad, M.H.; Badri, M.; Kashisaz, M.; Khaledi-Nasab, A.; Kroushawi, F. Facile one-pot phytosynthesis of magnetic nanoparticles using potato extract and their catalytic activity. *Starch-Staerke* **2016**, *68*, 796–804. [[CrossRef](#)]
40. Buazar, F.; Bavi, M.; Kroushawi, F.; Halvani, M.; Khaledi-Nasab, A.; Hossieni, S.A. Potato extract as reducing agent and stabiliser in a facile green one-step synthesis of ZnO nanoparticles. *J. Exp. Nanosci.* **2016**, *11*, 175–184. [[CrossRef](#)]
41. Koopi, H.; Buazar, F. A novel one-pot biosynthesis of pure alpha aluminum oxide nanoparticles using the macroalgae *Sargassum ilicifolium*: A green marine approach. *Ceram. Int.* **2018**, *44*, 8940–8945. [[CrossRef](#)]
42. Thommes, M.; Kaneko, K.; Neimark, A.V.; Olivier, J.P.; Rodriguez-Reinoso, F.; Rouquerol, J.; Sing, K.S.W. Physisorption of gases, with special reference to the evaluation of surface area and pore size distribution (IUPAC Technical Report). *Pure Appl. Chem.* **2015**, *87*, 1051–1069. [[CrossRef](#)]
43. Guellati, O.; Harat, A.; Momodu, D.; Dangbegnon, J.; Romero, T.; Begin, D. Electrochemical measurements of 1D/2D/3D Ni–Co bi-phase mesoporous nanohybrids synthesized using free-template hydrothermal method. *Electrochim. Acta* **2018**, *275*, 155–171. [[CrossRef](#)]
44. Liang, D.; Wu, S.; Liu, J.; Tian, Z.; Liang, C. Co-doped Ni hydroxide and oxide nanosheet networks: Laser-assisted synthesis, effective doping, and ultrahigh pseudocapacitor performance. *J. Mater. Chem. A* **2016**, *4*, 10609–10617. [[CrossRef](#)]
45. Lu, Y.; Chen, J.; Zhang, J.; Fu, C. Kinetic, isotherm and thermodynamic studies on the adsorption behavior of atrazine onto sheep manure-derived biochar. *Polish J. Environ. Stud.* **2019**, *28*, 2725–2733. [[CrossRef](#)]
46. El Hassani, K.; Beakou, B.H.; Kalnina, D.; Oukani, E.; Anouar, A. Effect of morphological properties of layered double hydroxides on adsorption of azo dye Methyl Orange: A comparative study. *Appl. Clay Sci.* **2017**, *140*, 124–131. [[CrossRef](#)]
47. Darmograi, G.; Prelot, B.; Layrac, G.; Tichit, D.; Martin-Gassin, G.; Salles, F.; Zajac, J. Study of Adsorption and Intercalation of Orange-Type Dyes into Mg–Al Layered Double Hydroxide. *J. Phys. Chem. C* **2015**, *119*, 23388–23397. [[CrossRef](#)]
48. Hoseinzadeh, E.; Samarghandi, M.R.; McKay, G.; Rahimi, N.; Jafari, J. Removal of acid dyes from aqueous solution using potato peel waste biomass: A kinetic and equilibrium study. *Desalin. Water Treat.* **2014**, *52*, 4999–5006. [[CrossRef](#)]
49. Samarghandy, M.R.; Hoseinzade, E.; Taghavi, M.; Hoseinzade, S. Solution using acid-treated biomass from potato. *BioResources* **2011**, *6*, 4840–4855.
50. Klett, C.; Barry, A.; Balti, I.; Lelli, P.; Schoenstein, F.; Jouini, N. Nickel doped Zinc oxide as a potential sorbent for decolorization of specific dyes, methyloange and tartrazine by adsorption process. *J. Environ. Chem. Eng.* **2014**, *2*, 914–926. [[CrossRef](#)]
51. Guan, T.; Fang, L.; Lu, Y.; Wu, F.; Ling, F.; Gao, J.; Hu, B.; Meng, F.; Jin, X. A facile approach to synthesize 3D flower-like hierarchical NiCo layered double hydroxide microspheres and their enhanced adsorption capability. *Colloids Surfaces A Physicochem. Eng. Asp.* **2017**, *529*, 907–915. [[CrossRef](#)]
52. Yu, X.; Zhang, G.; Xie, C.; Yu, Y.; Cheng, T.; Zhou, Q. Equilibrium, kinetic, and thermodynamic studies of hazardous dye neutral red biosorption by spent corncob substrate. *BioResources* **2011**, *6*, 936–949. [[CrossRef](#)]
53. Géraud, E.; Bouhent, M.; Derriche, F.; Leroux, F.; Prévot, V.; Forano, C. Texture effect of layered double hydroxides on chemisorption of Orange II. *J. Phys. Chem. Solids* **2007**, *68*, 818–823. [[CrossRef](#)]
54. Li, Q.; Chen, L.; Li, X.; Zhang, J.; Zhang, X.; Zheng, K.; Fang, F.; Zhou, H.; Tian, X. Effect of multi-walled carbon nanotubes on mechanical, thermal and electrical properties of phenolic foam via in-situ polymerization. *Compos. Part A Appl. Sci. Manuf.* **2016**, *82*, 214–225. [[CrossRef](#)]
55. Li, Z.; Yang, B.; Zhang, S.; Wang, B.; Xue, B. A novel approach to hierarchical sphere-like ZnAl-layered double hydroxides and their enhanced adsorption capability. *J. Mater. Chem. A* **2014**, *2*, 10202–10210. [[CrossRef](#)]
56. Lin, Y.; Zeng, Z.; Zhu, J.; Wei, Y.; Chen, S.; Yuan, X.; Liu, L. Facile synthesis of ZnAl-layered double hydroxide microspheres with core-shell structure and their enhanced adsorption capability. *Mater. Lett.* **2015**, *156*, 169–172. [[CrossRef](#)]
57. Tounsadi, H.; Metarfi, Y.; Barka, N.; Taleb, M.; Rais, Z. Removal of textile dyes by chemically treated sawdust of acacia: Kinetic and Equilibrium Studies. *J. Chem.* **2020**, 7234218. [[CrossRef](#)]
58. Maia, M.A.; Dotto, G.L.; Perez-Lopez, O.W.; Gutterres, M. Phosphate removal from industrial wastewaters using layered double hydroxides. *Environ. Technol.* **2020**, *42*, 3095–3105. [[CrossRef](#)]
59. Razzaghi-Asl, N.; Nasehi, P. Adsorption of Erythrosine and Red Carmosine dyes from aqueous solutions with CuO adsorbent: Kinetic and thermodynamic study. *Nord. Stud. Alcohol Drugs* **2016**, *6*, 21–31. [[CrossRef](#)]
60. Xu, D.; Zhang, L. Adsorption behavior of three-dimensional magnetic hollow porous Ni-ferrites microsphere for dyes removal. *J. Dispers. Sci. Technol.* **2018**, *39*, 423–430. [[CrossRef](#)]